

---

# Voxel-based Differentiable X-ray Rendering Improves Self-Supervised 3D CBCT Reconstruction

---

**Mohammadhossein Momeni**<sup>1,2\*</sup> **Vivek Gopalakrishnan**<sup>1,2\*</sup>

**Neel Dey**<sup>2</sup> **Polina Golland**<sup>2</sup> **Sarah Frisken**<sup>1</sup>

<sup>1</sup>Brigham and Women’s Hospital <sup>2</sup>MIT CSAIL

## Abstract

We present a self-supervised framework for Cone-Beam Computed Tomography (CBCT) reconstruction by directly optimizing a voxelgrid representation using physics-based differentiable X-ray rendering. Further, we investigate how the different formulations of X-ray image formation physics in the renderer affect the quality of 3D reconstruction and novel view synthesis. When combined with our regularized voxelgrid-based learning framework, we find that using an exact discretization of the Beer-Lambert law for X-ray attenuation in the renderer outperforms widely used iterative CBCT reconstruction algorithms, particularly when given only a few input views. As a result, we reconstruct high-fidelity 3D CBCT volumes from fewer X-rays, potentially reducing ionizing radiation exposure.

## 1 Introduction

CBCT reconstruction estimates internal 3D structure from multiple 2D X-ray projection images, typically acquired in a circular orbit about the subject (Fig. 1A). Current analytical and iterative solvers for CBCT reconstruction [1–3] fail when reconstructing from a limited number of 2D X-rays, typically prescribed to minimize radiation exposure to patients or reduce scan times. To this end, several neural fields-based methods aim to fill the need for sparse-view CBCT reconstruction [4–6].

However, these methods simplify the physics of the underlying X-ray image formation model (thus trading off fidelity) and rely on Transformer or MLP-hashgrid hybrid architectures [7] with high computational cost to reconstruct volumes. Furthermore, previous learning-based methods for CBCT reconstruction have predominantly been evaluated on synthetic X-ray datasets [8, 9], making it unclear if these architectures scale to real X-ray images. Despite their high performance on synthetic datasets, learning-based CBCT reconstruction methods have not seen widespread adoption in real-world tasks.

Instead of parameterizing the unknown volume as a neural network as in previous work [4–6], we propose to perform sparse-view reconstruction by directly optimizing a regularized voxelgrid representation [10] of a CBCT scan. Our self-supervised reconstruction framework has few tunable hyperparameters and is driven by a physics-based differentiable X-ray renderer that makes 3D CBCT reconstruction entirely compatible with autograd frameworks, enabling integration of popular regularizers (e.g., total variation norm [11]) and optimizers (e.g., Adam). We further investigate how different X-ray image formation models affect the quality of CBCT reconstruction: Siddon’s method, an exact model of the first-order effects in X-ray physics, and trilinear interpolation, a fast approximation of these phenomena. Whereas most existing learning-based reconstruction techniques use trilinear interpolation, we find that optimization with Siddon’s method leads to the highest quality reconstructions in the sparse-view regime. We evaluated our methods and many widely used baselines on an open dataset of more than 150,000 raw X-ray images from 42 subjects and found that our method outperforms popular CBCT reconstruction algorithms, albeit at the cost of longer runtimes.

---

\*Equal contribution. Correspondence to vivekg@mit.edu.

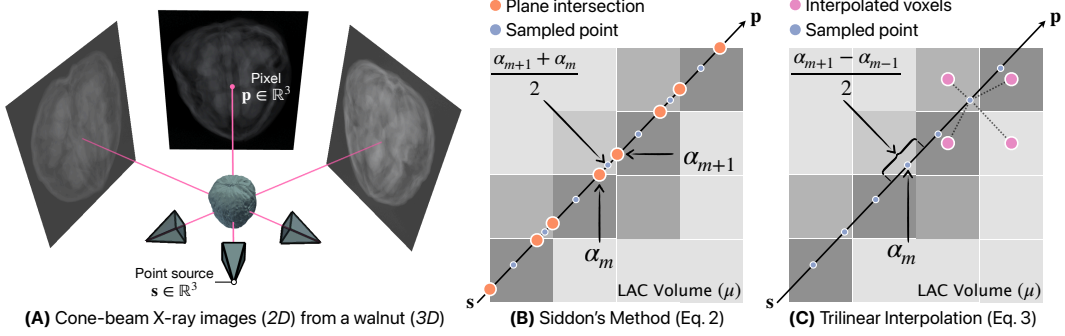


Figure 1: (A) In sparse-view CBCT reconstruction, a small number of X-ray images are acquired in a circular orbit about a subject. We compare two models of X-ray image formation when performing reconstruction via differentiable rendering: (B) Siddon’s method and (C) trilinear interpolation.

## 2 Methods

**Image Formation Model (Fig. 1).** Let  $\vec{r}(\alpha) = s + \alpha(p - s)$  with  $\alpha \in [0, 1]$  be a beam of photons cast through a heterogeneous medium from an X-ray source  $s \in \mathbb{R}^3$  to a pixel on the detector  $p \in \mathbb{R}^3$ . An X-ray image  $I$  quantifies the energy-weighted fraction of attenuated incident photons for every pixel in the detector, with the negative log intensity at  $p$  being governed by the Beer-Lambert law:

$$I_{\mu}(\vec{r}) = \int_{x \in \vec{r}} \mu(x) dx = \int_0^1 \mu(\vec{r}(\alpha)) \|\vec{r}'(\alpha)\| d\alpha = \|\vec{p} - \vec{s}\| \int_0^1 \mu(s + \alpha(\vec{p} - \vec{s})) d\alpha, \quad (1)$$

where  $\mu : \mathbb{R}^3 \rightarrow [0, \infty)$  represents the medium’s linear attenuation coefficients (LACs), a physical property proportional to the density at every point in space. In all practical settings,  $\mu$  is discretized onto a finite-resolution voxelgrid. Therefore, CBCT reconstruction via differentiable rendering requires numerical methods to compute Eq. (1) over a discrete volume of optimized LACs, denoted as  $\hat{\mu}$ , in a manner that is differentiable with respect to  $\hat{\mu}$ .

**Differentiable X-ray Rendering.** The first integration technique we consider is Siddon’s method [12], which exactly computes a discretized version of Eq. (1) as the sum of the LAC in every voxel on the path of  $\vec{r}$ , weighted by the intersection length of  $\vec{r}$  with each voxel:

$$I_{\hat{\mu}}(\vec{r}) = \|\vec{p} - \vec{s}\| \sum_{m=1}^{M-1} \hat{\mu} \left[ s + \frac{\alpha_{m+1} + \alpha_m}{2} (\vec{p} - \vec{s}) \right] (\alpha_{m+1} - \alpha_m), \quad (2)$$

where  $\{\alpha_1, \dots, \alpha_M\}$  parameterize the intersection of  $\vec{r}$  with the parallel planes comprising  $\hat{\mu}$ , and  $\hat{\mu}[\cdot]$  is an indexing operation that returns of the LAC of the intersected voxel (Fig. 1B). It was previously shown that Eq. (2) can be implemented in a completely differentiable manner [13]. Instead of computing every plane intersection, which scales cubically with the resolution of  $\hat{\mu}$ , we propose to approximate the Beer-Lambert law using interpolatory quadrature via the rectangular rule:

$$I_{\hat{\mu}}(\vec{r}) \approx \|\vec{p} - \vec{s}\| \sum_{m=1}^{M-1} \hat{\mu} [s + \alpha_m(\vec{p} - \vec{s})] \frac{(\alpha_{m+1} - \alpha_{m-1})}{2}, \quad (3)$$

where  $\{\alpha_1, \dots, \alpha_M\}$  parameterize  $M$  evenly spaced points along  $\vec{r}$  and  $\hat{\mu}[\cdot]$  represents trilinear interpolation (Fig. 1C). Trilinear interpolation is linear in  $M$  and thus faster than Siddon’s method.

**Differentiable CBCT Reconstruction.** Let  $\mathcal{R}$  represent the set of all photon beams cast in a set of 2D X-ray images of a subject, fully specifying the acquisition geometry. For each beam  $\vec{r} \in \mathcal{R}$ , let  $I_{\mu}(\vec{r}) \in [0, \infty)$  correspond to its ground truth pixel intensity. To reconstruct the unknown volume, we directly optimize the voxelgrid  $\hat{\mu}$  with the following photometric loss function:

$$\mathcal{L}(\hat{\mu}) = \frac{1}{|\mathcal{R}|} \sum_{\vec{r} \in \mathcal{R}} \|I_{\mu}(\vec{r}) - I_{\hat{\mu}}(\vec{r})\|_1 + \lambda_{\text{TV}} \text{TV}(\hat{\mu}), \quad (4)$$

where  $\|\cdot\|_1$  is the L1 norm and  $\text{TV}(\cdot)$  is the total variation norm, a commonly used regularizer that encourages reconstructed volumes to be piecewise constant [11]. Note that we implement  $I_{\hat{\mu}}$  as a differentiable renderer specifically to minimize  $\mathcal{L}$  using gradient-based optimization.

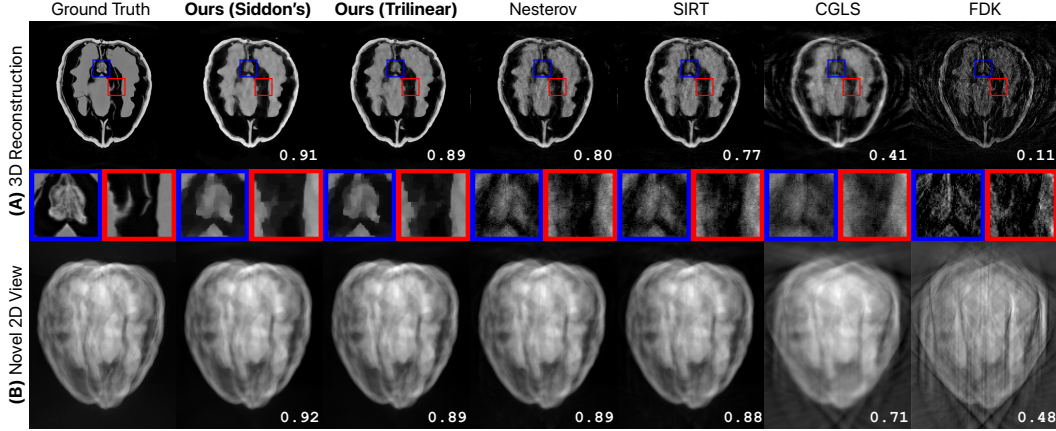


Figure 2: **(A)** CBCT reconstructions of an exemplar walnut from the test set using 30 input views across all methods, with Structural Similarity Index Measure (SSIM) for each 3D reconstruction and 2D novel view annotated. Blue insets highlight where our methods outperform the baselines, with sharper boundaries and fewer artifacts. Red insets indicate areas where all methods struggle, particularly in reconstructing thin structures. **(B)** Novel views rendered from these reconstructions are compared to a ground truth X-ray image from the low orbit, and similarly annotated with SSIM.

### 3 Experiments

**Dataset.** Commercial CT scanners typically do not provide access to raw projection data. Therefore, most sparse-view CBCT reconstruction methods are evaluated on artificial X-ray images simulated from existing 3D scans using computational models. Instead, we evaluated our proposed methods using an open dataset of real high-resolution X-ray images acquired from 42 walnuts [14]. For each walnut, 3,600 X-ray images were acquired across three circular orbits at different heights. Ground truth CBCT volumes were reconstructed using all images to produce  $501 \times 501 \times 501$  volumes at  $0.1 \text{ mm}^3$  isotropic spacing. At test-time, we reconstructed CBCT volumes using a sparse subset of X-ray images from only the middle orbit to replicate a typical cone-beam acquisition (Fig. 2A). In addition to comparing our 3D reconstructions to the high-resolution ground truth, we also measure how similar novel 2D views rendered from our reconstructed volumes were to real 2D X-ray images from the high and low orbits, which are not seen during optimization (Fig. 2B). All hyperparameters were tuned with a grid search over two subjects, and the remaining 40 were used as a held-out test set.

**Implementation Details.** We initialize  $\hat{\mu}$  as a voxelgrid of all zeros. As LACs are physically constrained to be nonnegative, we apply a shifted sigmoid activation function to  $\hat{\mu}$  prior to rendering. To optimize  $\hat{\mu}$ , we use the Adam optimizer with a starting step size of 1 and a linear step size that decays to 0 over the number of iterations. We used 100 and 50 iterations for Siddon’s method and trilinear interpolation, respectively. Due to memory constraints, the maximum batch size achievable for each renderer was  $|\mathcal{R}| = 5.5 \times 10^5$  for Siddon’s method and  $|\mathcal{R}| = 2 \times 10^6$  for trilinear interpolation. Finally, we set  $\lambda_{\text{TV}} = 25$  for Siddon’s method and  $\lambda_{\text{TV}} = 15$  for trilinear interpolation. Reported runtimes are measured using a single RTX A6000 GPU.

**Baselines.** We compare against GPU-accelerated implementations of four classical CBCT reconstruction algorithms from the ASTRA Toolbox [15]: Feldkamp-Davis-Kress (FDK) [1], Conjugate Gradient Least Squares (CGLS) [2], Simultaneous Iterative Reconstruction Technique (SIRT) [3], and Nesterov-Accelerated Gradient Descent (Nesterov) [14]. These baselines were highly sensitive to the number of iterations used during optimization. Based on grid searches to maximize their performance, we ran CGLS for 20 iterations, SIRT for 500 iterations, and Nesterov for 50 iterations.

**Results.** We tested the performance of our proposed methods and baseline approaches in the sparse-view regime, reconstructing 40 walnuts with the number of input views ranging from  $\{5, 10, 15, \dots, 60\}$ . To evaluate the quality of these 3D reconstructions and novel 2D views, we compute the following image fidelity scores: Structural Similarity Index Measure (SSIM), Peak Signal-to-Noise Ratio (PSNR), Pearson’s Correlation Coefficient (PCC), and Mean Squared Error (MSE). Across all performance metrics and numbers of views, our differentiable rendering ap-

Table 1: Quantitative comparison for 3D reconstruction from 30 views averaged over the 40 test walnuts. Our methods excel in their reconstruction quality, however, they require more runtime than traditional baselines. The number of iterations for each method was tuned and increasing the runtime beyond what is reported here resulted in *worse* reconstructions. Metrics are reported as *mean (std)*.

	SSIM ( $\uparrow$ )	PSNR ( $\uparrow$ )	$MSE \times 10^{-6} (\downarrow)$	PCC ( $\uparrow$ )	Runtime ( $\downarrow$ )
FDK [1]	0.259 (0.098)	24.88 (3.59)	279 (15)	0.62 (0.02)	<b>0.8 sec</b>
CGLS [2]	0.607 (0.119)	32.71 (3.57)	46.1 (2.8)	0.86 (0.01)	4.2 sec
SIRT [3]	0.878 (0.062)	37.45 (3.65)	15.6 (2.3)	0.96 (0.01)	76 sec
Nesterov [14]	0.897 (0.052)	38.28 (3.64)	12.9 (1.9)	0.96 (0.01)	2.7 min
<b>Trilinear (ours)</b>	0.944 (0.031)	40.45 (3.58)	7.57 (0.82)	<b>0.98 (0.00)</b>	20.6 min
<b>Siddon (ours)</b>	<b>0.950 (0.024)</b>	<b>40.46 (3.58)</b>	<b>7.56 (0.84)</b>	<b>0.98 (0.00)</b>	44.9 min
<b>Trilinear w/o TV (ours)</b>	0.85 (0.05)	30.94 (3.62)	71.5 (8.0)	0.81 (0.01)	20.0 min
<b>Siddon w/o TV (ours)</b>	0.70 (0.07)	16.74 (3.52)	1837 (236)	0.25 (0.01)	40.8 min

proaches outperform classical CBCT reconstruction techniques by appreciable margins (Tab. 1), with the greatest gains in sparse-view settings.

In 3D reconstruction, Siddon’s method provides a modest improvement over trilinear interpolation at the expense of requiring nearly  $2\times$  the runtime due to its increased complexity (Tab. 1). However, when rendering novel 2D views from these reconstructed volumes, the advantage of Siddon’s method is evident in Fig. 3B. Projections rendered from volumes reconstructed with Siddon’s method have consistently higher fidelity than those produced by trilinear interpolation or any baseline method.

For both differentiable rendering methods, regularization via TV norm leads to high-quality reconstructions. However, as the ablation study in Tab. 1 shows, removing the TV norm has a far greater impact on Siddon’s method. This is because while Siddon’s method exactly computes the line integral in the Beer-Lambert law, trilinear interpolation allows rendered pixel intensities to be influenced by voxels not directly intersected by  $\vec{r}$  (Fig. 1). This is advantageous as it enables ground truth pixels to provide self-supervision to many more voxels, preventing the overfitting seen with Siddon’s method. Furthermore, this behavior is an approximation of second-order effects such as X-ray scatter, something that Siddon’s method does not model.

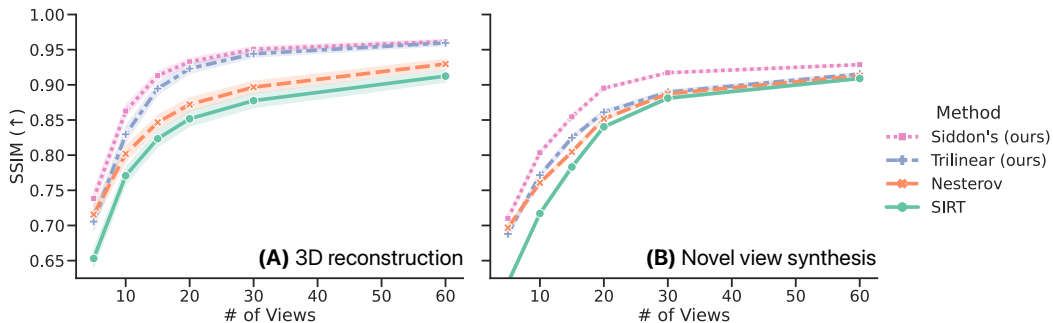


Figure 3: Quality of (A) reconstructed 3D volumes and (B) novel 2D views over a range of sparse 2D acquisitions. For comparison, we show the top-performing baselines, Nesterov and SIRT.

## 4 Conclusions

This study proposes a modular framework for performing CBCT reconstruction with differentiable X-ray rendering. In comparing multiple X-ray image formation models combined with our regularized reconstruction framework, we find that Siddon’s method results in the highest-quality reconstructions at the expense of higher runtimes. Our preliminary results naturally suggest several potential areas for future work. For example, incorporating a more realistic X-ray image formation model (e.g., Siddon’s method) into learning-based methods may yield compounding benefits. Furthermore, as our physics-based reconstruction framework is fully differentiable, priors beyond TV regularization can be easily incorporated for specialized imaging applications such as vascular imaging.

**Acknowledgments.** This work was supported in part by NIH NIBIB NAC P41EB015902, NIH NINDS U19NS115388, NIH NIBIB 5T32EB001680-19, and NIH R01EB034223.

## References

- [1] Lee A Feldkamp, Lloyd C Davis, and James W Kress. Practical cone-beam algorithm. *Journal of the Optical Society of America A*, 1(6):612–619, 1984.
- [2] Malena Sabaté Landman, Ander Biguri, Sepideh Hatamikia, Richard Boardman, John Aston, and Carola-Bibiane Schönlieb. On Krylov methods for large-scale CBCT reconstruction. *Physics in Medicine & Biology*, 68(15):155008, 2023.
- [3] Jens Gregor and Thomas Benson. Computational analysis and improvement of SIRT. *IEEE Transactions on Medical Imaging*, 27(7):918–924, 2008.
- [4] Ruyi Zha, Yanhao Zhang, and Hongdong Li. NAF: neural attenuation fields for sparse-view CBCT reconstruction. In *International Conference on Medical Image Computing and Computer-Assisted Intervention*, pages 442–452. Springer, 2022.
- [5] Darius Rückert, Yuanhao Wang, Rui Li, Ramzi Idoughi, and Wolfgang Heidrich. NeAT: Neural adaptive tomography. *ACM Transactions on Graphics (TOG)*, 41(4):1–13, 2022.
- [6] Yiqun Lin, Zhongjin Luo, Wei Zhao, and Xiaomeng Li. Learning deep intensity field for extremely sparse-view CBCT reconstruction. In *International Conference on Medical Image Computing and Computer-Assisted Intervention*, pages 13–23. Springer, 2023.
- [7] Thomas Müller, Alex Evans, Christoph Schied, and Alexander Keller. Instant neural graphics primitives with a multiresolution hash encoding. *ACM Transactions on Graphics (TOG)*, 41(4):1–15, 2022.
- [8] Yuanhao Cai, Jiahao Wang, Alan Yuille, Zongwei Zhou, and Angtian Wang. Structure-aware sparse-view X-ray 3d reconstruction. In *Proceedings of the IEEE/CVF Conference on Computer Vision and Pattern Recognition*, pages 11174–11183, 2024.
- [9] Johannes Leuschner, Maximilian Schmidt, Daniel Otero Baguer, and Peter Maass. LoDoPaB-CT, a benchmark dataset for low-dose computed tomography reconstruction. *Scientific Data*, 8(1):109, 2021.
- [10] Cheng Sun, Min Sun, and Hwann-Tzong Chen. Direct voxel grid optimization: Super-fast convergence for radiance fields reconstruction. In *Proceedings of the IEEE/CVF Conference on Computer Vision and Pattern Recognition*, pages 5459–5469, 2022.
- [11] Leonid I Rudin, Stanley Osher, and Emad Fatemi. Nonlinear total variation based noise removal algorithms. *Physica D: Nonlinear Phenomena*, 60(1-4):259–268, 1992.
- [12] Robert L Siddon. Fast calculation of the exact radiological path for a three-dimensional CT array. *Medical Physics*, 12(2):252–255, 1985.
- [13] Vivek Gopalakrishnan and Polina Golland. Fast auto-differentiable digitally reconstructed radiographs for solving inverse problems in intraoperative imaging. In *Workshop on Clinical Image-Based Procedures*, pages 1–11. Springer, 2022.
- [14] Henri Der Sarkissian, Felix Lucka, Maureen van Eijnatten, Giulia Colacicco, Sophia Bethany Coban, and Kees Joost Batenburg. A cone-beam X-ray computed tomography data collection designed for machine learning. *Scientific Data*, 6(1):215, 2019.
- [15] Wim Van Aarle, Willem Jan Palenstijn, Jeroen Cant, Eline Janssens, Folkert Bleichrodt, Andrei Dabravolski, Jan De Beenhouwer, K Joost Batenburg, and Jan Sijbers. Fast and flexible X-ray tomography using the ASTRA toolbox. *Optics Express*, 24(22):25129–25147, 2016.